Protein Science (1998), 7:2359–2373. Cambridge University Press. Printed in the USA.

pH-Induced conformational changes of membrane-bound influenza hemagglutinin and its effect on target lipid bilayers

CAMERON GRAY AND LUKAS K. TAMM

Department of Molecular Physiology and Biological Physics, University of Virginia Health Sciences Center, P.O. Box 10011, Charlottesville, Virginia 22906-0011

(RECEIVED May 30, 1998; ACCEPTED July 20, 1998)

Abstract

Influenza virus hemagglutinin (HA) has served as a paradigm for both pH-dependent and -independent viral membrane fusion. Although large conformational changes were observed by X-ray crystallography when soluble fragments of HA were subjected to fusion-pH conditions, it is not clear whether the same changes occur in membrane-bound HA, what the spatial relationship is between the conformationally changed HA and the target and viral membranes, and in what way HA perturbs the target membrane at low pH. We have taken a spectroscopic approach using an array of recently developed FTIR techniques to address these questions. Difference attenuated total reflection FTIR spectroscopy was employed to reveal reversible and irreversible components of the pH-induced conformational change of the membrane-bound bromelain fragment of HA, BHA. Additional proteolytic fragments of BHA were produced which permitted a tentative assignment of the observed changes to the HA_1 and HA_2 subunits, respectively. The membrane-bound HA_1 subunit undergoes a reversible conformational change, which most likely involves the loss of a small proportion of β-sheet at low pH. BHA was found to undergo a partially reversible tilting motion relative to the target membrane upon exposure to pH 5, indicating a previously undescribed hinge near the anchoring point to the target membrane. Time-resolved amide H/D exchange experiments revealed a more dynamic (tertiary) structure of membrane-bound BHA and its HA_2, but not its HA_1, subunit. Finally BHA and, to a lesser degree, HA_1 perturbed the lipid bilayer of the target membrane at the interface, as assessed by spectral changes of the lipid ester carbonyl groups. These results are discussed in the context of a complementary study of HA that was bound to viral membranes through its transmembrane peptide (Gray C, Tamm LK, 1997, *Protein Sci 6*:1993–2006). A distinctive role for the HA_1 subunit in the conformational change of HA becomes apparent from these combined studies.

Keywords: conformational change; influenza hemagglutinin; lipid-protein interaction; membrane fusion; polarized ATR Fourier transform infrared spectroscopy

Recent studies on viral membrane fusion proteins have highlighted the importance of influenza hemagglutinin (HA) as the structural paradigm for both pH-dependent and -independent viral membrane fusion (Bullough et al., 1994; Fass et al., 1996; Chan et al., 1997; Weissenhorn et al., 1997). Sequence and structural information on the fusion proteins of influenza, human immunodeficiency, and Moloney murine leukemia viruses has suggested that the dynamics of α-helical coiled coils in response to either pH or receptor binding are essential in the mechanism of protein-mediated membrane fusion. However, the dynamics of coiled coil refolding primarily explain how the putative fusion peptides (typically, amphipathic, ~20 residue peptides residing at the N-terminus of the membrane-anchored polypeptide chain) of the viral fusion proteins are extruded and made accessible to the target membrane. The insertion of the fusion peptide into the target membrane is a necessary, but not sufficient, step in the catalysis of membrane fusion. In the case of influenza HA, studies have implicated conformational changes in parts of the protein distant from the stem coiled coil region in regulating the extent, kinetics, and pH dependence of the mem-

Reprint requests to: Lukas K. Tamm, Department of Molecular Physiology and Biological Physics, University of Virginia Health Sciences Center, P.O. Box 10011, Charlottesville, Virginia 22906-0011; e-mail: lkt2e@virginia.edu.

Abbreviations: ATR, attenuated total reflection; BHA, bromelain fragment of HA; BHA_2, trypsin fragment of BHA; EM, electron microscopy; FTIR, Fourier transform infrared; HA, hemagglutinin; HEPES, *N*-(2-hydroxyethyl)-piperazine-*N'*-(2-ethanesulfonic acid); MES, 2-(4-morpholino)-ethanesulfonic acid; PAGE, polyacrylamide gel electrophoresis; PATR, polarized ATR; POPC, 1-palmitoyl-2-oleoyl-3-*sn*-phosphatidylcholine; POPG, 1-palmitoyl-2-oleoyl-3-*sn*-phosphatidylglycerol; SDS, sodium dodecylsulfate; $TBHA_2$, trypsin/thermolysin fragment of BHA; TLCK, N^a-p-tosyl-L-lysine-chloromethylketone; WB, working buffer (5 mM HEPES, pH 7.4, 150 mM NaCl).

brane fusion reaction (Daniels et al., 1985; Godley et al., 1992; Kemble et al., 1992; Steinhauer et al., 1996; Gray & Tamm, 1997). Experimental elucidation of how these conformational changes contribute to the catalysis of membrane fusion may provide a fuller description of how a fusion pore is assembled, and, critically, the nature of the commitment step leading from initial lipid mixing and pore flickering to full contents mixing (Chernomordik et al., 1995).

In addition to serving as a paradigm for viral fusion proteins, influenza HA represents a class of membrane proteins for which there is high-resolution crystallographic information regarding their ectodomains, i.e., soluble fragments produced by proteolytic cleavage near the membrane surface. Many such proteins serve as cell surface receptors, and conformational changes in response to ligand binding are ultimately to be transmitted across the cell membrane. There are two caveats to extrapolating from crystallographic studies of soluble fragments of membrane proteins to their mechanisms of action: (1) it is unclear whether such fragments assume the same structure in solution as they do attached to their membrane anchor at the membrane surface; and (2) it is unclear how the information contained in ligand engagement is transduced through the ectodomain and eventually across the membrane.

In a previous study, we have examined the secondary structure, orientation, and dynamical changes of full-length influenza HA in its membrane-bound form using difference attenuated total reflection (ATR)-FTIR spectroscopy (Gray & Tamm, 1997). Specifically, we investigated the conformational changes imposed on HA by low pH in the presence and absence of bound target membranes. To assign structural changes to different parts of the polypeptide chain various proteolytic fragments, which all contained the transmembrane anchoring peptide, were generated and compared with complete HA. In the present study, which is complementary to this previous work, we examine the pH dependence of the interaction of soluble fragments of influenza HA with model target membranes. The bromelain-solubilized ectodomain of HA (BHA) and two of its fragments, BHA_2 (consisting of residues 1–27 of HA_1 and 1–175 of HA_2) and HA_1 (consisting of residues 28–328 of HA_1), are prepared and their secondary structures, dynamic structures, orientations relative to the membrane, and their effects on the structure of the lipid bilayer are investigated by ATR-FTIR spectroscopy as a function of pH. All these experiments are carried out on supported membranes in physiological buffers. The fragments used and compared in this and our previous (Gray & Tamm, 1997) study are shown in Figure 1. Collectively, these studies indicate an important, previously underestimated structural role of the HA_1 chain in HA-mediated membrane fusion.

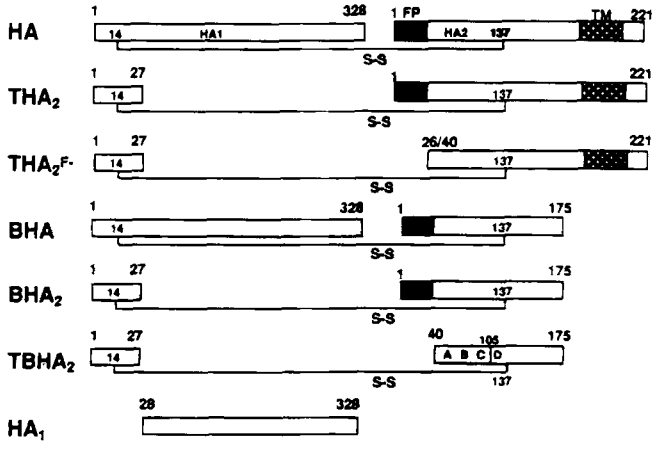

Fig. 1. Overview of the polypeptide arrangement of influenza strain X:31 HA and derived fragments used in this and previous work. The membrane-anchored species HA, THA_2, and THA_2^{F-} were characterized in a previous study (Gray & Tamm, 1997). The characterization of the soluble fragments BHA, BHA_2, and HA_1 and their binding to target membranes are described here. Crystal structures are known for BHA at neutral pH, $TBHA_2$ at low pH, and HA_1 at intermediate pH. FP, fusion peptide; TM, transmembrane peptide.

Results

Soluble fragments of the membrane-released ectodomain of HA, BHA (Fig. 1) were prepared by limited trypsin digestion. The SDS polyacrylamide gels shown in Figures 2A and 2B document the pH dependence of the BHA trypsinization reaction, and the ensuing isolation of the resulting fragments by sucrose density gradient centrifugation, respectively. The starting material, BHA, was loaded on lane 2 of the gel of Figure 2A. HA_1 and BHA_2 run at about 58 and 26 kDa, respectively. Lanes 3, 4, and 5 of this gel show the proteolytic fragments of BHA produced by incubation with trypsin at increasing pH, i.e., 6.5, 7.5, and 8.0, respectively. At progressively higher pH values, trypsin-sensitive sites near the N-terminus of the HA_2 chain become accessible, as has been documented previously (Ruigrok et al., 1988). This pH dependence is especially evident in lanes 4 and 5 of Figure 2A, where the relative distribution of the BHA_2 and $TBHA_2$ (i.e., BHA_2, which lacks the fusion peptide) products are markedly different. Because we wanted to measure the conformation of membrane-bound BHA, and since the interaction of the influenza HA_2 chain with target membranes is mediated solely by the fusion peptide (Durrer et al., 1996), it was important to find conditions under which the BHA_2 fragment could be produced in large excess over the $TBHA_2$ fragment. Figure 2A demonstrates that this condition is fulfilled at pH <7.5. Lanes 3–5 also demonstrate the partial cleavage of HA_1 into HA_1(28–224), denoted HA1*, and HA_1(225–328), denoted HA1**. The latter is only seen in the higher percentage gel of Figure 2B. After incubation for less than 15 min at room temperature and a fairly low enzyme:substrate ratio (1:30), more than 50% of the HA_1 chains are cleaved, irrespective of the pH.

The various tryptic fragments of BHA that were produced by proteolysis at pH 6.5 (sample of Fig. 2A, lane 3) were separated and purified by sucrose density gradient centrifugation. Fractions collected from the continuous sucrose gradient were loaded on the gel presented in Figure 2B. Lanes 3 and 4 show purified BHA_2 and HA_1, respectively. Lane 5 demonstrates that the two HA_1 subfragments migrate to the same density in the continuous sucrose gradient. We did not attempt to further separate these products. For reference, the starting material, BHA, is shown in lane 2.

pH-dependent conformational changes in BHA, BHA_2, and HA_1

The natural ligand for influenza HA is sialic acid as, for example, presented by gangliosides on the extracellular surface of host cell plasma membranes. However, the application of infrared spectroscopy, particularly in the conformation-sensitive amide I region, precludes the use of gangliosides, because they contain amide groups whose absorptions overlap with the corresponding protein

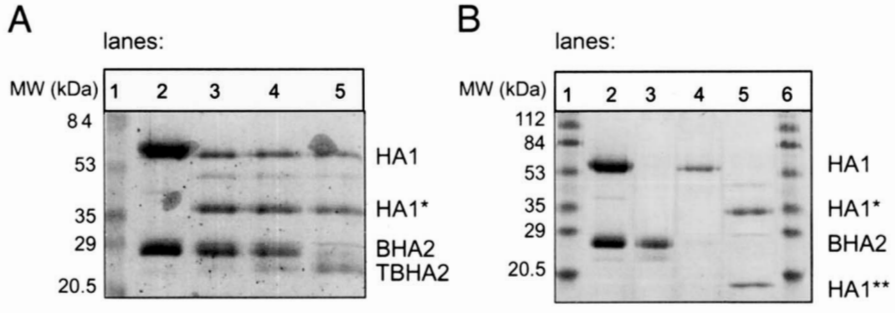

Fig. 2. (**A**) SDS-PAGE analysis of the pH dependence of the proteolysis of BHA by trypsin and (**B**) the subsequent purification of the tryptic fragments of BHA. In **A** (12.5% acrylamide), lane 2 is intact BHA and lanes 3–5 are the products of 20, 40, and 60 min incubations of BHA with trypsin at pH 6.5, 7.5, and 8.0, respectively, at room temperature and an enzyme:substrate ratio of 1:30 (w/w). In **B** (16% acrylamide), lane 2 is intact BHA and lanes 3–5 contain fractions collected from a sucrose gradient separating the products of the reaction shown in lane 3 of **A**. Lane 5 of the gel in **B** resolves both HA_1 trypsin breakdown products, HA_1^* and HA_1^{**}, whereas HA_1^{**} is lost from the gel in **A** because of the lower percentage of acrylamide in this gel.

absorption bands. For this reason, supported bilayers composed of POPC:POPG in the outer leaflets were used here as target membranes. The negatively charged lipid POPG mimics the electrostatic environment of sialic acid, promoting binding of BHA and its fragments to supported lipid bilayers. In Figure 3, ATR-FTIR spectra of BHA, BHA_2, and HA_1 bound to supported lipid bilayers composed of POPC:POPG (1:1) in the outer leaflets are compared in the amide I′ region. Similar spectra were obtained with bilayers whose outer leaflets were composed of POPC:POPG (4:1), indicating that the charge density had no appreciable effect on the observed amide I′ bands. Spectra of the corresponding pure lipid bilayers were used as references to produce the spectra displayed in Figure 3, which therefore represent IR bands of the respective membrane-bound proteins without any major contributions from the membranes. The amide I′ bands of BHA and HA_1 are very broad and asymmetric with a peak at ~1,637 cm^{-1}. These bands are probably dominated by β-structures as expected from the crystal structures of these two molecules (Wilson et al., 1981; Bizebard et al., 1995) and are consistent with usual secondary structure assignments from FTIR spectroscopy (Krimm & Bandekar, 1986; Surewicz et al., 1993; Jackson & Mantsch, 1995). Again using the known crystal structures and standard secondary structure assignments as guidelines, the broad shoulders at higher wavenumbers likely arise from random coil and α-helix for BHA and random coil, turns, and antiparallel β-sheets for HA_1. No attempts have been made to curve-fit these spectra or to quantify the relative amounts of secondary structure. The FTIR spectrum of BHA_2 is more symmetric and centered at ~1,648 cm^{-1}. These features are consistent with a large proportion of helical structure, potentially in the form of a helical coiled coil (Heimburg et al., 1996; Reisdorf & Krimm, 1996), as may be anticipated on the basis of the crystal structure of $TBHA_2$ (Bullough et al., 1994).

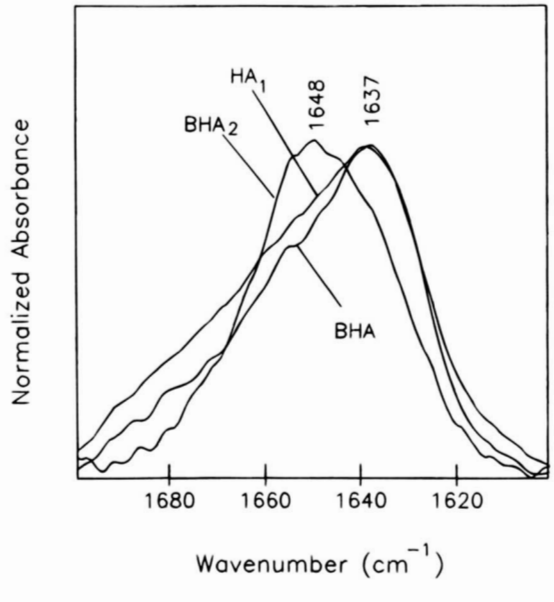

Fig. 3. Parallel polarized ATR-FTIR absorbance spectra in the amide I′ region for BHA, BHA_2, and HA_1 bound to supported bilayers of POPC/POPC:POPG (1:1) at pH 7.4.

Difference spectroscopy is more reliable than band-shape analysis for observing secondary structure *changes* as a function of experimental conditions (Gray & Tamm, 1997; Tamm & Tatulian, 1997). Therefore, we present in Figure 4 a gallery of difference ATR-FTIR spectra for membrane-bound BHA, BHA_2 and HA_1 as a function of pH. Figures 4A, 4B, and 4C show the effects of acidification (top spectra), followed by reneutralization (bottom spectra), for BHA, BHA_2, and HA_1, respectively. These spectra address the conformational changes induced by pH in BHA and its fragments bound to target membranes, and the reversibility of these changes in the presence of target membranes. The spectra of Figure 4A suggest that some of the acid-induced shifts in secondary structure of membrane-bound BHA are reversible, whereas others are irreversible. The positive band in the top spectrum near 1,665 cm^{-1} implies that turn structures are more prevalent at neutral pH and the negative band near 1,620 cm^{-1} suggests that low pH induces an increase of aggregated β-strand structure in BHA (Jackson & Mantsch, 1995). Only part of the bottom spectrum of Figure 4A is a mirror image of the top spectrum (reflected about the $\Delta A = 0$ axis), indicating an at least partially irreversible conformational change upon reneutralization. Even more difference absorbance intensity appears in the region that is normally assigned to turns, indicating a further loss of these structures as the pH is returned to neutral. In addition, a gain in β-sheet (region

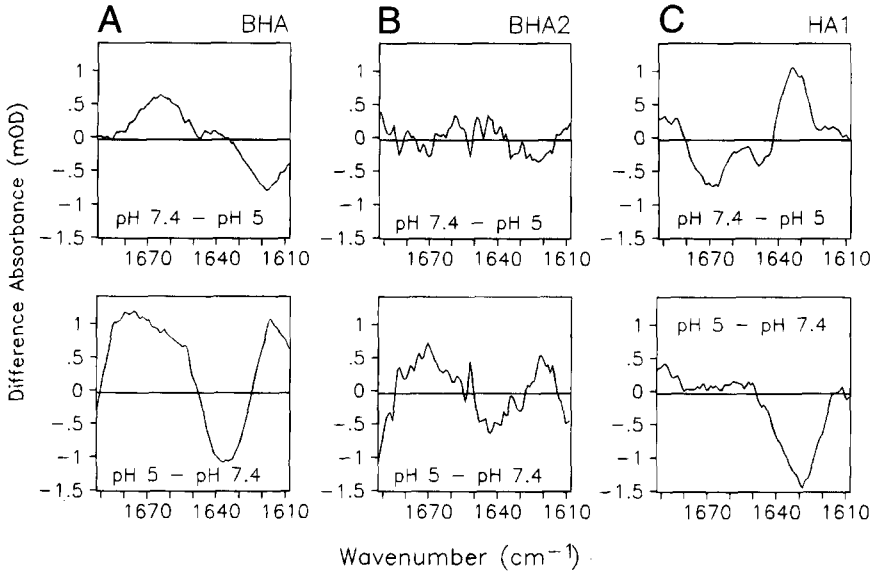

Fig. 4. Sequences of difference ATR-FTIR spectra (parallel polarized) for (**A**) BHA, (**B**) BHA_2, and (**C**) HA_1 bound to supported bilayers of POPC/POPC:POPG corresponding to the differences imposed by acidification and subsequent neutralization. The pH sequence was 7.4 →5 →7.4. Difference spectra pH 7.4–pH 5 (top panels) and pH 5–pH 7.4 (bottom panels) are shown. All spectra are the averages of three difference spectra measured with three independent samples.

around 1,635 cm^{-1}) and a reversible loss of the aggregated β-strand structures (region around 1,620 cm^{-1}) appears to occur upon reneutralization.

In contrast to BHA, BHA_2 does not change much its secondary structure when the pH is lowered from 7.4 to 5 (Fig. 4B, top spectrum). However, some small changes may occur when the pH is returned to 7.4. Although these changes appear to be reproducible in three independent identical experiments, the signal-to-noise in the BHA_2 difference spectra is much lower than in the BHA and HA_1 difference spectra even after signal averaging. Therefore, we conclude that the membrane-bound BHA_2 conformation is essentially insensitive to pH. Complementary experiments with HA_1 are presented in Figure 4C. The most significant change occurs in the 1,630–1,635 cm^{-1} spectral region, which is normally assigned to β-sheets (Jackson & Mantsch, 1995). This change is largely reversible: some of the β-sheet is lost when this fragment is converted to its pH 5 structure, but a similar proportion of β-sheet is refolded upon reneutralization. Based on the magnitude of the observed relative changes, we estimate that about 15–25 residues participate in this reversible conformational change. Although a similar increase in β-sheet is observed in BHA upon the pH 5 → pH 7.4 change, many of the other spectral changes of BHA_2 and HA_1 are not additive and superposition of the respective difference spectra does not simply restore the BHA difference spectra. This is not surprising if one recalls that BHA had to be briefly exposed to low pH to produce the HA_1 and BHA_2 fragments. If the conformational change of BHA is partially irreversible as shown in Figure 4A and elsewhere (Doms et al., 1985; White & Wilson, 1987), we cannot expect simple additivity of the spectra shown in Figures 4B and 4C to restore those of Figure 4A.

pH-Dependent orientational changes in BHA, BHA_2, and HA_1

Polarized ATR-FTIR experiments yield information on the orientation of secondary structure elements relative to the plane of the membrane (Tamm & Tatulian, 1997). Table 1 lists dichroic ratios

Table 1. *Changes in dichroic ratios and order parameters of membrane-bound BHA and its fragments upon acidification and reneutralization*

	Dichroic ratio, R^{ATR}			Change, ΔR^{ATR}		Change, ΔS_{oH}[a]	
Species	pH 7.4	pH 5	pH 7.4	pH 7.4 →5	pH 5 →7.4	pH 7.4 →5	pH 5 →7.4
BHA	2.90 ± 0.14	2.47 ± 0.15	2.75 ± 0.23	−0.42 ± 0.09	0.28 ± 0.19	−0.94 ± 0.39	0.63 ± 0.86
BHA_2	2.44 ± 0.60	2.20 ± 0.56	2.18 ± 0.46	−0.25 ± 0.11	−0.03 ± 0.12	−0.32 ± 0.29	−0.03 ± 0.34
HA_1	1.62 ± 0.14	1.35 ± 0.17	1.38 ± 0.20	−0.27 ± 0.06	0.03 ± 0.03	—	—

[a]The fraction of residues in ordered helices was estimated from the crystal structures of BHA and $TBHA_2$ to be 117/503 = 0.233 in BHA and 92/202 = 0.455 in BHA_2.

and order parameters obtained from PATR-FTIR experiments on BHA and HA_1 bound to supported lipid bilayers composed of POPC:POPG (4:1) in the outer leaflet, and BHA_2 bound to bilayers composed of POPC:POPG (1:1) in the outer leaflet. As noted previously (Gray & Tamm, 1997), the relative standard deviations of repeated experiments are smaller for dichroic ratio and order-parameter *changes* than for the respective parent values. For BHA and its fragments, acidification invariably lowers the dichroic ratio and, therefore, the order parameter. Since the order parameter can vary between 1.0 for an orientation of the helices parallel to the bilayer normal and -0.5 for an orientation of the helices parallel to the plane of the bilayer, the observed change of $\Delta S = -0.94$ represents a significant tilt of the helices of BHA to orientations less perpendicular to the bilayer surface. A smaller tilt in the same direction is observed for BHA_2 ($\Delta S = -0.32$). Both of these molecules contain significant proportions of α-helical structure and, therefore, the reported order parameters refer to changes of oriented helix orientation. The interpretation of the dichroic ratio decrease observed for HA_1 as a function of pH is less straightforward because this protein is mainly composed of antiparallel β-sheet (Bizebard et al., 1995). Two order parameters obtained from two independent measurements would be required to fully describe the orientation of β-sheets (Rodionova et al., 1995; Marsh, 1997). The change in molecular orientation of BHA is partially reversible (pH 5 $\rightarrow$7.4, $\Delta S = 0.63$) whereas that of BHA_2 ($\Delta S = -0.03$) is essentially irreversible.

Dynamic structure of BHA, BHA_2, and HA_1

Measurements of amide hydrogen exchange rates can be effectively used to probe the dynamic structure of proteins (Englander & Mayne, 1992). These exchange rates are sensitive to tertiary contacts in the protein as well as to the stability and exposure to solvent of individual secondary structures. It is known that in HA the receptor binding site and most of the antigenic epitopes are located in HA_1 while HA_2 is the major contributor to the membrane fusion activity of HA. Since the HA_2 chain is further known to undergo large conformational changes involving secondary structure changes and changes in tertiary contacts upon exposure to low pH, we wanted to know whether these changes could be probed by altered amide H/D exchange rates and whether experimental conditions such as membrane binding or the separation of the HA_1 and HA_2 chains would affect the observed H/D exchange behavior. Thus, amide H/D exchange experiments on BHA, BHA_2, and HA_1 could potentially provide important new insight into the mechanism of HA and a comparison of such measurements between the three molecules could shed new light on the dynamic coupling between the HA_1 and HA_2 chains.

Amide hydrogen exchange is conveniently measured in IR spectroscopy by an isotope-induced shift of the amide I and II band positions when the protein is transferred from H_2O into D_2O solutions. In our H/D exchange experiments, we examined the solvent accessibility of protein backbone amide protons in a window between 2 min and 22 h after the exchange of H_2O with D_2O buffers. Surface-exposed non-hydrogen-bonded amide hydrogens are expected to exchange within the first 2 min and are therefore not detected in these experiments. Figure 5 shows time-resolved difference spectra in the amide I region of membrane-bound BHA (Fig. 5A,D), BHA_2 (Fig. 5B,E), and HA_1 (Fig. 5C,F), induced by solvent exchange. The sets of difference spectra displayed in each panel were generated by subtracting the spectrum corresponding to the most deuterated state (i.e., 22 h post-exchange) from spectra collected at progressively later time points as one moves vertically toward the horizontal line drawn at $\Delta A = 0$. In a control experiment shown in Figure 5G, we incubated HA in D_2O for 40 h (to exchange all exchangeable amide hydrogens) and then recorded IR spectra at several time intervals for 22 h. No significant changes were observed in difference spectra calculated from these control experiments, indicating that (1) our instrument produced a stable baseline for at least 22 h and (2) no measurable further H/D exchange took place after such a long exposure to D_2O buffer. Since the frequencies at which particular residues absorb are sensitive to their structural context, the temporal decays of difference spectra like those shown in Figure 5A–F contain information pertaining to the rates of exchange for characteristic secondary structure elements. It is apparent from the spectral shape changes of Figure 5 that the rates of exchange are different at different frequencies. For instance, the spacing between successive spectra in the negative and positive bands is distinctly different, suggesting differences in the rates of exchange for residues absorbing in these two regions of the spectrum. Similarly, the spacings between spectra in Figures 5A and 5D vary, implying that different H/D exchange rates obtain at neutral and acidic pH for BHA. These differences with respect to subunit composition and pH are further analyzed by plotting the time courses of the decays at selected spectral positions.

Figure 6 displays the time courses of difference absorbance for membrane-bound BHA, BHA_2, and HA_1 at three selected frequencies at pH 7.4 and 5. The curves of the three fragments are overlaid in each panel; the panels on the left correspond to H/D exchange at pH 7.4 and the ones on the right correspond to H/D exchange at pH 5. The data of Figure 6 were then fit by a nonlinear least-squares algorithm to double-exponential functions as described in Materials and methods. In a few cases where fits to two exponentials were not significantly better than fits to a single exponential, single-exponential fits were used. The solid lines in Figure 6 represent the respective best fits to the experimental data. The resulting fit parameters, including confidence intervals, are listed in Table 2. We first describe common features of the observed time courses and subsequently highlight some features that are different between the three HA fragments and their respective conformations at neutral and low pH.

Most of our H/D exchange time courses are characterized by two time constants, one on the order of 10 to 30 min (k_1^{-1}) and one on the order of 4 to 6 h (k_2^{-1}). The amplitudes of the faster decay are typically about two to three times those of the slower decays, i.e., they contribute about 66–75% to the total observable exchanging amide hydrogens. This behavior is found, for example, for the 1,680 and the 1,660 band of BHA at pH 7.4 (with the 1,660 band decaying at the slower end for both k_1 and k_2). However, the 1,635 band of BHA is reasonably well characterized with a single slow decay process occurring over about 6 h. At pH 5, the overall H/D exchange is faster at all frequencies than at pH 7.4, but the rates decrease in the same order at both pH values: 1,680 > 1,660 > 1,635 cm^{-1}. Using our tentative assignments from above, this would indicate that turns and loops exchange faster than general helices, which in turn exchange faster than β-structures and possibly helices in coiled coils. Irrespective of these assignments, and based on the increased observed H/D exchange rates, the pH 5 structure of BHA appears more dynamic than the pH 7.4 structure.

The dynamic behavior of BHA_2 is different from that of BHA in two respects. First, the band at 1,680 cm^{-1} (tentatively assigned to

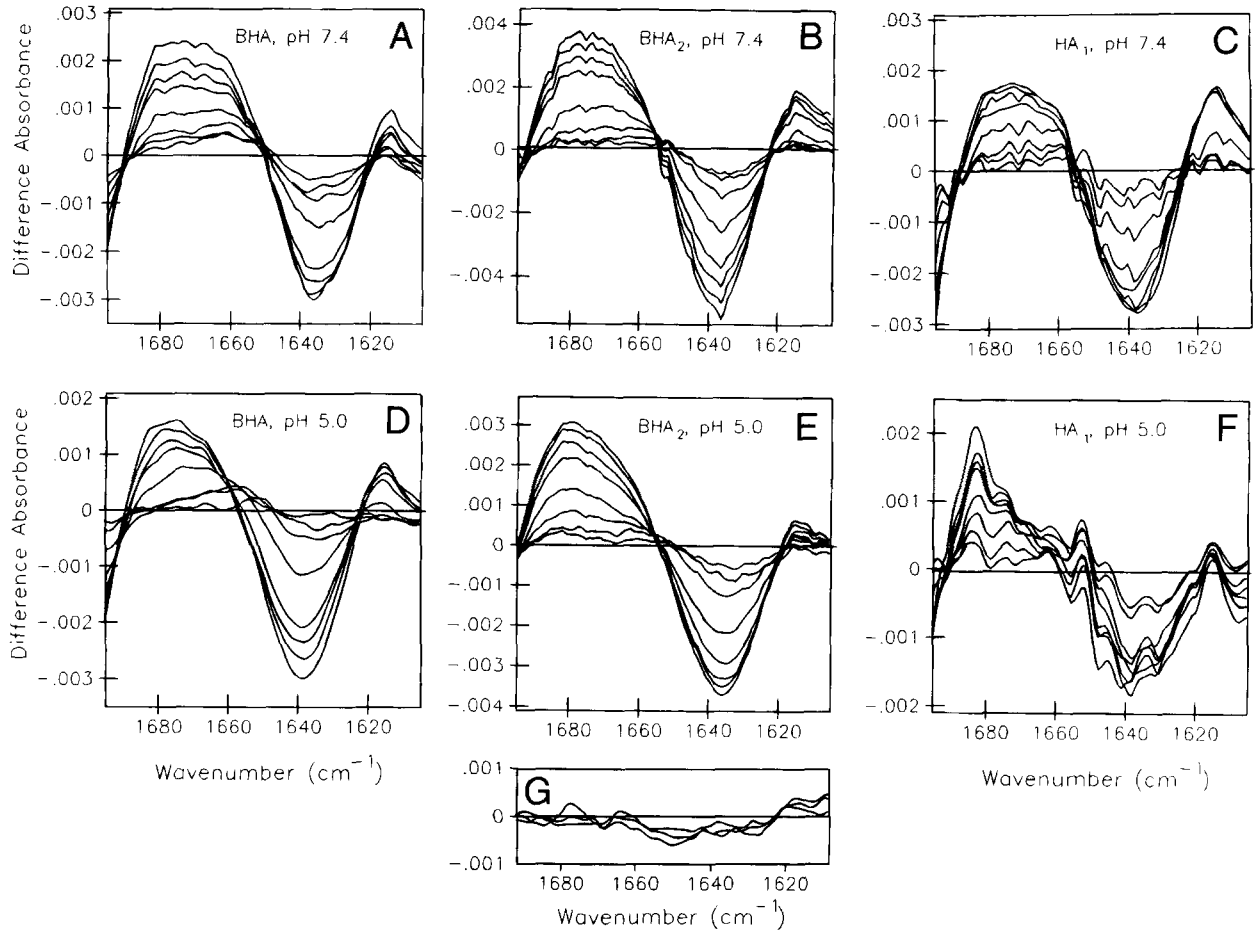

Fig. 5. Difference ATR-FTIR spectra showing time-dependent changes in the amide I′ region after substitution of an H_2O for a D_2O buffer for membrane-bound (**A, D**) BHA, (**B, E**) BHA_2, and (**C, F**) HA_1 at (**A–C**) pH 7.4 and (**D–F**) pH 5. The difference spectra were calculated using the spectrum obtained after 22 h of exposure to D_2O as the reference. Moving vertically toward the line drawn at $\Delta A = 0$, the difference spectra correspond to 2 min, 5 min, 18 min, 47 min, 2:15 h, 4:45 h, 7:15 h, and 9:45 h after solvent exchange. (**G**) A control experiment is shown in which a sample of membrane-incorporated HA was exposed to D_2O buffer for 40 h before spectra were taken at 43, 52, and 62 h and subtracted from the 40 h spectrum.

turns and loops) exchanges faster at pH 7.4, and slower at pH 5. At 1,660 cm^{-1} the overall rates are similar at the two pH values and the band at 1,635 cm^{-1} (tentatively assigned to β-structures and/or coiled coils) again exchanges faster at pH 5 than at pH 7.4 as was observed in BHA. This could mean that in BHA_2 turns rigidify, but β-sheets and/or coiled coils become more flexible at pH 5. Compared to the other structures, HA_1 exchanges its amide hydrogens more slowly at all three characteristic frequencies. In fact, at 1,660 and 1,640 cm^{-1} the faster component was absent altogether in these decay curves. (These spectra were also noisier, which is part of the reason why double-exponential fits gave no statistical improvement over single-exponential fits.) The loops and turns (band at 1,680 cm^{-1}) of HA_1 become more exposed to amide hydrogen exchange than the other secondary structures, which appear to exchange very slowly in a fashion that is not well characterized by single- or double-exponential functions in the observed time window. A possible reason for our failure to obtain data of the same quality for HA_1 as for the other two fragments could be that HA_1 forms reversible aggregates of β-sheet (or other secondary) structures at membrane surfaces at pH 5 (see above).

Effects of protein adsorption/insertion on the lipid bilayer structure

Figure 7 shows the band contours of the lipid ester carbonyl stretching vibration as a function of increasing BHA:lipid ratios (Fig. 7A) and increasing HA_1:lipid ratios (Fig. 7B). This band is known to be composed of two bands, a component at ~1,740 cm^{-1} and a component at ~1,727 cm^{-1}, which are ascribed to "free" and hydrogen-bonded (to water) carbonyl groups, respectively (Blume et al., 1988; Lewis et al., 1994). The carbonyl groups of both the *sn*-1 and *sn*-2 acyl chains contribute approximately equally to these component bands. The bottom spectra in both Figures 7A and 7B correspond to the ester carbonyl bands of POPC:POPG (4:1) in plain lipid bilayers. The subsequent spectra represent 6–8-fold and 8–10-fold increases in protein:lipid ratio as one progresses toward the top spectra in Figures 7A and 7B, respectively. On visual inspection, the topmost spectra in both panels suggest that a change in the distribution of component bands underlying the carbonyl stretching vibration has occurred relative to the case for pure POPC:POPG (4:1). This effect is particularly striking for the case

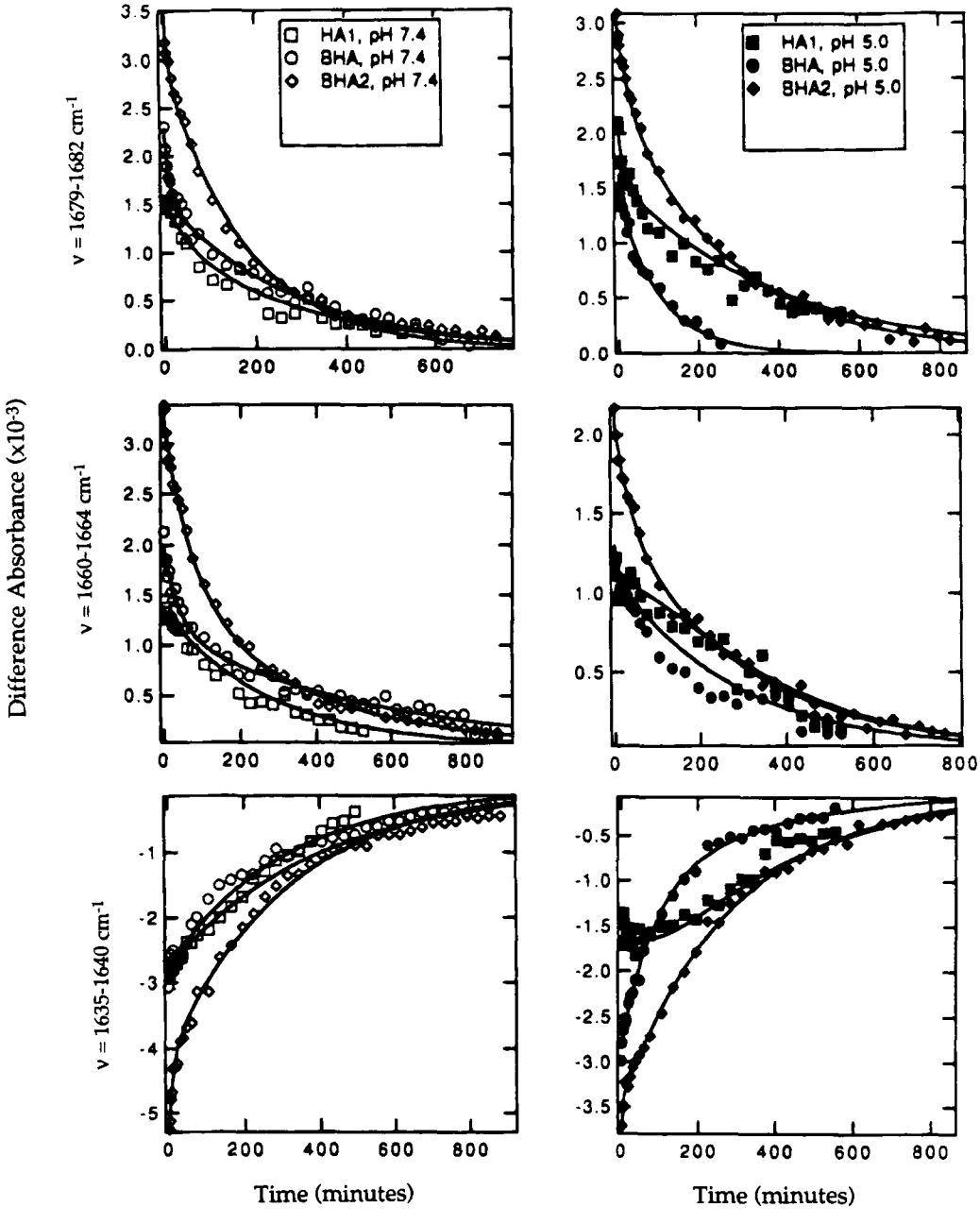

Fig. 6. Kinetics of H/D exchange measured at 1,679–1,682 cm^{-1} (top panels), 1,660–1,664 cm^{-1} (middle panels), and 1,635–1,640 cm^{-1} (bottom panels), at pH 7.4 (left panels) and pH 5.0 (right panels) for (○,●) BHA), (◇,◆) BHA_2, and (□,■) HA_1 bound to supported POPC:POPG bilayers. The difference absorbances were calculated by subtracting the spectrum measured after 22 h of exposure to D_2O as the reference. Each time course was fit with a single or double exponential function (solid lines) as described in Materials and methods. The fit parameters are listed in Table 2.

of BHA (Fig. 7A), where the hydrated lower frequency component band increasingly dominates the appearance of the lipid carbonyl band contour.

Table 3 lists dichroic ratios and order parameters for the lipid carbonyl stretching and the methylene stretching vibrations as a function of protein adsorption and pH. The former relates to the molecular order of both acyl-chain carbonyl groups in the interfacial region of the lipid bilayer and the latter reflects the degree of acyl-chain order in the hydrophobic core of the lipid bilayer. In most of the cases reported in Table 3, protein adsorption does not appear to significantly affect the lipid order in the bilayer. However, there is one notable exception: BHA shifts the dichroic ratio of the lipid ester carbonyl band to significantly lower values, an effect which is observed at neutral and low pH. Interestingly, the dichroic ratios and order parameters of the methylene stretching band are not significantly altered as a result of BHA binding to the planar lipid bilayers. Similarly, BHA_2 does not significantly affect the lipid dichroic ratio. Neither BHA nor BHA_2 changed the frequency positions of the symmetric and antisymmetric methylene stretching bands (data not shown).

Table 2. *Analysis of the amide H/D exchange behavior of BHA, BHA_2, and HA_1, at neutral and low pH at three selected frequencies by fits of the data of Figure 6 to double (or single) exponential functions*[a]

	1,679–1,682 cm^{-1}		1,660–1,664 cm^{-1}		1,635–1,640 cm^{-1}	
	a_1 (mOD) k_1 ($\times 10^2$ min^{-1})	a_2 (mOD) k_2 ($\times 10^3$ min^{-1})	a_1 (mOD) k_2 ($\times 10^3$ min^{-1})	a_2 (mOD) k_2 ($\times 10^3$ min^{-1})	a_1 (mOD) k_1 ($\times 10^2$ min^{-1})	a_2 (mOD) k_2 ($\times 10^3$ min^{-1})
BHA						
pH 7.4						
Amplitude	1.6 (1.5, 1.6)[b]	0.7 (0.7, 0.8)	1.2 (1.1, 1.2)	0.8 (0.8, 0.9)	—	−3.4 (−3.3, −3.5)
Rate	9.1 (7.2, 11.1)	3.7 (3.5, 3.9)	2.6 (2.2, 3.0)	1.9 (1.7, 2.0)	—	4.1 (3.8, 4.5)
pH 5.0						
Amplitude	—	1.5 (1.4, 1.5)	1.1 (1.1, 1.1)	0.2 (0.2, 0.3)	−1.1 (−1.0, −1.3)	−1.7 (−1.6, −1.7)
Rate	—	9.8 (9.2, 10.3)	10.0 (4.9, 20.3)	3.5 (3.3, 3.7)	1.2 (1.1, 1.3)	2.8 (2.6, 3.1)
BHA_2						
pH 7.4						
Amplitude	3.0 (2.9, 3.0)	0.8 (0.7, 0.9)	1.6 (1.5, 1.7)	1.6 (1.5, 1.7)	−4.1 (−4.0, −4.2)	−1.2 (−1.0, −1.3)
Rate	12.7 (9.4, 17.2)	5.8 (5.5, 6.0)	1.4 (1.2, 1.5)	2.9 (2.7, 3.0)	7.5 (5.9, 9.9)	3.2 (3.0, 3.3)
pH 5.0						
Amplitude	2.3 (2.3, 2.4)	0.7 (0.6, 0.7)	1.5 (1.4, 1.6)	0.6 (0.5, 0.6)	−3.4 (−3.4, −3.4)	−0.4 (−0.3, −0.5)
Rate	3.3 (2.6, 3.6)	3.6 (3.5, 3.7)	2.7 (2.2, 3.4)	3.4 (3.3, 3.6)	24.8 (16.6, 36.4)	3.3 (3.2, 3.4)
HA_1						
pH 7.4						
Amplitude	1.1 (0.9, 1.3)	0.4 (0.3, 0.7)	—	1.3 (1.3, 1.4)	—	−2.8 (−2.7, −2.9)
Rate	2.0 (1.3, 3.6)	3.4 (2.7, 3.8)	—	3.7 (3.6, 3.8)	—	2.1 (1.7, 2.5)
pH 5.0						
Amplitude	1.6 (1.5, 1.7)	0.5 (0.5, 0.7)	2.0 (1.8, 2.1)	−0.9 (−0.07, −1.0)	−3.1 (−2.9, −3.2)	1.5 (1.4, 1.6)
Rate	9.5 (6.7, 14.4)	2.6 (2.5, 2.8)	0.8 (0.6, 1.0)	3.7 (3.3, 3.9)	0.9 (0.8, 1.0)	3.0 (2.9, 3.2)

[a]Amplitudes and rate constants were found using the Nelder–Mead simplex algorithm (Johnson & Frasier, 1985).
[b]All numbers in parentheses are the confidence intervals for one standard deviation found using a Monte Carlo simulation with 800 cycles (Straume & Johnson, 1992).

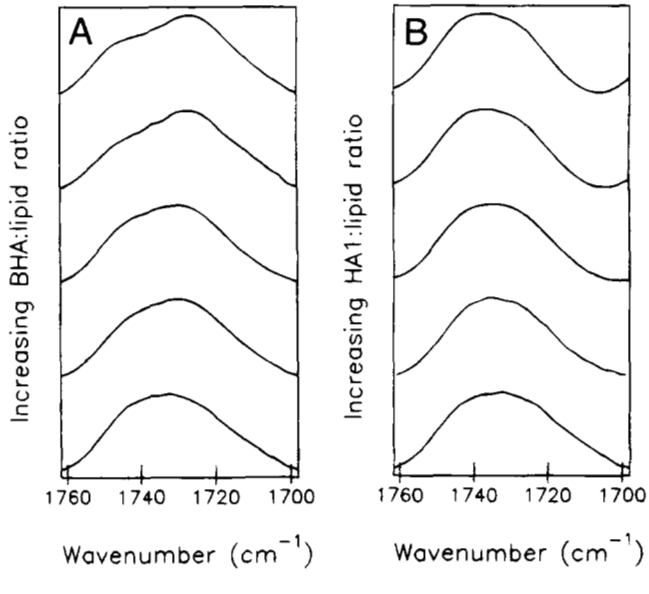

Fig. 7. Parallel polarized ATR-FTIR spectra showing the lipid ester carbonyl stretching band of POPC:POPG (4:1) lipid bilayers for increasing concentrations of (**A**) bound BHA and (**B**) bound HA_1. Estimated molar protein:lipid ratios increase from about 1:800 to about 1:125 from bottom to top in **A** and from about 1:800 to about 1:90 in **B**.

Discussion

The main goal of the present study was to elucidate in detail the conformational changes that take place when membrane-bound BHA is subjected to the pH of fusion and to assign specific roles to the HA_1 and HA_2 chains and their mutual interactions in this reaction. This was achieved by selective removal of one or the other of the two polypeptide chains from BHA by limited proteolysis and the subsequent measurement of difference ATR-FTIR spectra of the resulting BHA fragments in their membrane-bound forms before and after pH changes from pH 7.4 to pH 5 and back to pH 7.4.

BHA was bound to planar target membranes through the fusion peptide (and, possibly, electrostatic interactions) in all of our studies. The structures of BHA and BHA_2/$TBHA_2$ in the absence of target membranes have been previously studied by X-ray crystallography, electron microscopy, and circular dichroism spectroscopy (Wilson et al., 1981; Skehel et al., 1982; Ruigrok et al., 1986, 1988; Wharton et al., 1988; Bullough et al., 1994). Similar structural information has been obtained for the HA_1 subunit in the context of BHA and alone, i.e., bound to a monoclonal antibody (Wilson et al., 1981; Bizebard et al., 1995). The pH-induced conformational changes arising in the HA_1 chain are known to involve the exposure of previously protected antigenic epitopes and proteolytic sites (Skehel et al., 1982; White & Wilson, 1987), and it is

Table 3. *Dichroic ratios and order parameters of membrane lipids as a result of binding of BHA and its fragments and in response to acidification and reneutralization*

	Dichroic ratio, R^{ATR}				Order parameter, S		
	pH 7.4	pH 5	pH 7.4		pH 7.4	pH 5	pH 7.4
Pure POPC:POPG (4:1) bilayers							
$R^{ATR}_{C=O}$	1.73 ± 0.05	1.65 ± 0.06	—	$S_{C=O}$	0.00 ± 0.02	−0.03 ± 0.03	—
R^{ATR}_{CH2}	1.66 ± 0.07	1.63 ± 0.08	—	S_{CH2}	0.05 ± 0.06	0.07 ± 0.07	—
Pure POPC:POPG (1:1) bilayers							
$R^{ATR}_{C=O}$	1.63 ± 0.08	1.59 ± 0.09	—	$S_{C=O}$	−0.04 ± 0.04	−0.05 ± 0.04	—
R^{ATR}_{CH2}	1.55 ± 0.11	1.53 ± 0.13	—	S_{CH2}	0.14 ± 0.10	0.16 ± 0.12	—
BHA bound to (4:1) bilayers							
$R^{ATR}_{C=O}$	1.48 ± 0.08	1.32 ± 0.14	1.47 ± 0.05	$S_{C=O}$	−0.10 ± 0.04	−0.19 ± 0.08	−0.11 ± 0.03
R^{ATR}_{CH2}	1.65 ± 0.01	1.55 ± 0.02	1.63 ± 0.02	S_{CH2}	0.05 ± 0.01	0.14 ± 0.02	0.07 ± 0.02
BHA_2 bound to (1:1) bilayers							
$R^{ATR}_{C=O}$	1.70 ± 0.06	1.62 ± 0.07	1.68 ± 0.15	$S_{C=O}$	−0.01 ± 0.03	−0.04 ± 0.04	−0.01 ± 0.06
R^{ATR}_{CH2}	1.56 ± 0.09	1.54 ± 0.05	1.57 ± 0.07	S_{CH2}	0.13 ± 0.08	0.15 ± 0.05	0.12 ± 0.06
HA_1 bound to (4:1) bilayers							
$R^{ATR}_{C=O}$	1.64 ± 0.04	1.60 ± 0.04	1.65 ± 0.02	$S_{C=O}$	−0.03 ± 0.02	−0.05 ± 0.02	−0.03 ± 0.01
R^{ATR}_{CH2}	1.63 ± 0.03	1.55 ± 0.10	1.62 ± 0.06	S_{CH2}	0.07 ± 0.02	0.14 ± 0.09	0.08 ± 0.05

known that the introduction of intersubunit disulfide bonds in the HA_1 subunit inhibits HA-mediated membrane fusion (Godley et al., 1992; Kemble et al., 1992). However, except for some electron microscopic evidence for shape changes, the structural details of the conformational change of membrane-bound BHA have not been previously studied.

Based on our experiments, six major conclusions are reached regarding the pH-induced conformational change of membrane-bound BHA:

1. Membrane-bound BHA at pH 5 contains an increased amount of aggregated β-strands and an decreased proportion of turn structures compared to membrane-bound BHA at neutral pH.
2. The conformational change of membrane-bound BHA is partially, but not completely, reversible; aggregated strand formation appears to be reversible, whereas the loss of turns is irreversible.
3. Membrane-bound BHA_2, which is produced after a brief preexposure to pH 5, is largely inert to pH-induced conformational changes.
4. Membrane-bound HA_1 undergoes a pH-induced conformational change that appears to involve the reversible loss of β-sheet conformation of about 15–25 residues at low pH.
5. BHA tilts its molecular axis toward the plane of the membrane upon exposure to low pH. This tilt requires the presence of the HA_1 chain (which itself does not change its orientation to a large extent); BHA_2 tilts much less than BHA.
6. As evidenced by amide H/D exchange, the low-pH structure of membrane-bound BHA is more dynamic than its neutral pH structure. This increased flexibility of low-pH BHA can be attributed mainly to the HA_2 subunit; in contrast, membrane-bound HA_1 may become more rigid at low pH than at neutral pH.

Each of these results will be discussed in more detail in the following.

Reversible and irreversible conformational changes of membrane-bound BHA

BHA presumably binds through electrostatic interactions to supported bilayers of POPC:POPG (4:1). The negatively charged POPG mimics the charge of the physiological ligand of HA, sialic acid. The difference spectra of membrane-bound BHA shown in Figure 4A suggest that acidification is accompanied by the induction of increased aggregated β-strand and decreased turn content, evidenced by the negative band centered at ~1,620 cm^{-1} and the positive band at ~1,665 cm^{-1}. These assignments as well as those below are only used as guidelines. Although amide I band positions are good indicators of secondary structures in a very large number of proteins, the correlations are not absolute and there are some notable exceptions to the general rules (Surewicz et al., 1993; Jackson & Mantsch, 1995). For example, most α-helices absorb in the 1,650–1,660 cm^{-1} region, but it has been found recently that helical coiled coils also contribute to a spectral region around 1,630–1,640 cm^{-1} which is normally assigned to β-sheet (Heimburg et al., 1996; Reisdorf & Krimm, 1996). The changes in secondary structure of BHA induced by acidification and subsequent reneutralization are partially reversible. Reneutralization is accompanied by a loss of aggregated structure (positive band centered at ~1,620 cm^{-1} in the bottom spectrum) and a further loss of turns and perhaps standard helices (broad feature between 1,650–1,690 cm^{-1}), and an increase in β-sheet and/or coiled coil helices (negative band at 1,630–1,640 cm^{-1} in the bottom spectrum). Although several aspects of the conformational change of HA have

long been known to be irreversible, other aspects of the conformational change have been previously reported to be reversible under appropriate conditions (Tatulian & Tamm, 1996; Korte et al., 1997).

In contrast to BHA, there is no identifiable conformational change imposed on membrane-bound BHA_2 by acidification (Fig. 4B, top spectrum). One might conclude, therefore, that most of the conformational change detected in BHA is attributed to the HA_1 subunit and its interaction with HA_2. However, there are two caveats that prohibit drawing conclusions from a direct extrapolation of the BHA_2 data to the structure of the HA_2 subunit in BHA. First, BHA_2 has gone through a brief pH 5 → pH 7.4 cycle during its preparation (before trypsinization), whereas BHA has not. Therefore, irreversible components of the conformational change of BHA_2 are not expected to be seen in this experiment. Second, the conformational changes in BHA may not be the sum of the conformational changes of its parts. Mutual interactions between the two polypeptide chains may well contribute to the overall changes as seen, for example, in the analysis of the molecular tilt of BHA (see below). The bottom spectrum of Figure 4B suggests that reneutralization may still cause some structural changes in BHA_2. This result is in apparent contradiction with the notion that $TBHA_2$ assumes its lowest energy conformation at acidic pH and that it, therefore, would assume the same conformation at neutral and acidic pH in the absence of the constraining contacts with the HA_1 subunit (Chen et al., 1995). There are two reasons why these conclusions reached for $TBHA_2$ may warrant amendment for BHA_2. First, previous studies have implicated an influence of the fusion peptide, especially when bound to target membranes, on the structure and function of HA (Gething et al., 1986; Ruigrok et al., 1986; Steinhauer et al., 1995; Gray & Tamm, 1997). BHA_2 retains the fusion peptide and $TBHA_2$ does not. Second, $TBHA_2$ exists as a trimer in solution and BHA_2, when produced by trypsinization of BHA, exists in solution as a rosette with several trimers. Therefore, when BHA_2 binds to the target membrane through insertion of the fusion peptide, several BHA_2 trimers are in close proximity to one another. Interactions between neighboring trimers, which are also anticipated from functional measurements of membrane fusion (Blumenthal et al., 1996; Danieli et al., 1996), may influence the conformational change experienced by this molecule.

Figure 4C displays evidence for a reversible pH-induced conformational change which involves unfolding and refolding of about 15–25 residues of β-sheet in the HA_1 subunit in its membrane-bound form. This is the first time secondary structure transitions as a function of pH have been directly demonstrated in HA_1. The crystal structure of isolated HA_1 subunits (in complex with an antibody) has been solved; no significant changes from the structure of HA_1 in BHA were observed under the employed crystallization conditions at pH 6.0 (Bizebard et al., 1995). The reversible changes we observe could, therefore, be caused by membrane binding and/or the lower pH (5.0) that was used in our studies. The quaternary structure of the HA_1 domains is known to change during membrane fusion because the introduction of disulfide bonds in inter-subunit contacts between adjacent HA_1 subunits inhibits HA-mediated membrane fusion and severely impairs the ability of HA to undergo the acid-induced conformational change (Godley et al., 1992; Kemble et al., 1992). Recent work from this laboratory also suggests a role for the HA_1 subunit in regulating efficacy, pH dependence, and conformational changes involved in HA-mediated membrane fusion (Gray & Tamm, 1997). Two further studies have implicated, although more indirectly, conformational changes in HA_1 to acquire fusion competence of HA: The exposure of conformationally sensitive antibody epitopes correlates with membrane fusion (White & Wilson, 1987) and a large number of influenza mutants with altered fusion-pH profiles map in the HA_1 chain (Daniels et al., 1985). In summary, we surmise that changes in the conformation of the HA_1 subunit play an important role in HA-mediated membrane fusion.

A second hinge for tilting HA near the membrane-inserted fusion peptide

The IR-dichroic measurements reported in Table 1 indicate a relatively large negative change in the order parameter, which is a measure of the orientational distribution of the oriented helices of BHA in response to acidification. Since the order parameter, defined as $S = (3\langle\cos^2\theta\rangle - 1)/2$ (θ = angle between molecular axis and membrane normal), is 1.0 for molecules with a perfect perpendicular alignment to the plane of the membrane and -0.5 for molecules that are perfectly aligned with the plane of the membrane, a -0.9 change in order parameter represents a large angular change with most BHA molecules tilting toward the plane of the membrane. This angular change of BHA is partially reversible when the pH is returned to pH 7.4 ($\Delta S = +0.6$). Although in the same direction, the corresponding angular change for BHA_2 is much smaller ($\Delta S = -0.3$) and may not be reversible ($\Delta S = 0$, but note ~0.3 standard deviations on forward and backward reactions). The orientational changes of BHA and BHA_2 are reminiscent of previous results obtained with two membrane-embedded analogues, HA and THA_2, which showed low pH-induced order-parameter changes of -0.9 and -0.1, respectively (Gray & Tamm, 1997). In both cases, the molecules containing both polypeptide chains, but not their HA_2 derivatives, tilt by a large angle toward the membrane surface upon exposure to low pH. The HA_1 subunit, which does not contain ordered helices, appears to modulate the tilting motion of both molecules. Although measurements of the helix order parameter cannot determine whether all three helices in a trimeric coiled coil remain associated or splay apart as a result of this conformational change, we favor a stable trimeric association for energetic reasons (Tatulian et al., 1995; Chen et al., 1995). Despite this apparent analogy between HA and BHA in terms of their tilting toward the membrane plane at low pH, it should be noted that the two molecules are differently constrained. BHA and its fragments are constrained by electrostatic interaction of the sialic acid binding pocket with the negatively charged membranes, and in some cases, the inserted fusion peptides. However, the membrane-embedded HA species are constrained by the transmembrane domain and, when target membranes are bound, the fusion peptides and/or the sialic acid binding pockets. Therefore, we conclude that *two* hinges exist in HA, one at the base of HA near the transmembrane peptide, i.e., near the viral membrane, and the other at the top of HA near the attachment of the fusion peptide to the target membrane. The second hinge at the top of HA could either be located within the HA molecule or, alternatively, could be caused by different interactions of BHA with the target membrane at neutral and low pH, resulting in a different orientation of BHA on the membrane surface.

The low-pH structure of membrane-bound HA, particularly HA_2, is more dynamic than its neutral-pH structure

The amide H/D experiments presented in Figures 5 and 6 and Table 2 address the dynamic structure of BHA and its fragments

at neutral and acidic pH. Amide hydrogen exchange itself is known to be highly pH-dependent, but most of this dependence concerns exchange in an unfolded polypeptide and occurs on a time scale of 10 s or faster at the pH values in question (Englander & Mayne, 1992). We have investigated amide H/D exchange in a temporal window between approximately 2 min and 22 h, where exchange depends entirely on the probability of opening a tightly hydrogen-bonded secondary structure and the exposure of the corresponding amides to solvent. Thus, our measured H/D exchange kinetics reflect differences in the dynamic structures of BHA and its fragments at neutral or acidic pH. Since amide I band positions potentially contain information on the secondary structures that give rise to them, an analysis of the H/D exchange rates at different frequencies can be used to assess differences in the dynamics of different secondary structures. However, this assessment is qualitative only because of the overlap of different secondary structure band positions and because of the comparatively small, $\sim$10 cm^{-1}, isotope shift of the amide I band. For example, if a band at 1,650 cm^{-1} shifts upon H/D exchange by 10 cm^{-1} with the same rate as a band at 1,640 cm^{-1}, the net result at 1,640 cm^{-1} would be no change. Therefore, rates measured at the central frequencies in the amide I region may arise as composites of several kinetic processes and would only set a lower limit on the actual exchange rates. Rates measured in the wings of the overall amide I band are less sensitive to this problem. Despite these caveats, we analyzed the H/D exchange kinetics in three spectral regions to qualitatively compare differences of the dynamic behavior of BHA, BHA_2, and HA_1 at neutral and acidic pH. Although the amide II band is more sensitive than the amide I band to isotope exchange, we have not attempted to analyze this band in this work because secondary structure assignments are less well documented for the amide II band and because of spectral overlap of the H-O-D bending and amide II′ modes (see also Gray & Tamm, 1997).

One major result of the H/D exchange data of Table 2 is that the frequency component at 1,660–1,665 cm^{-1} of BHA_2 decays with time constants of 71 min at pH 7.4 and 37 min at pH 5. The corresponding values for BHA are 38 and 10 min at pH 7.4 and 5, respectively. Similar conclusions, although not as clear-cut, can be reached about the exchange rates in the other spectral regions for BHA and BHA_2. Thus, it appears that the structures of BHA and BHA_2 become more dynamic, i.e., more flexible, at low pH. This result is consistent with a recent spin-labeling study on an expressed portion representing the coiled coil of HA_2, in which it was shown that the region of the coiled coil that has undergone the loop-to-coil transition is relatively flexible (Kim et al., 1996). Also, mutations to single prolines in this region, which would be expected to partially destabilize the coiled coil, did not abolish the fusion activity of HA (Qiao et al., 1998), which indicates that a rigid coiled coil is not a requirement for fusion. The H/D exchange kinetics of HA_1 are rather slow and not well represented by one or two exponentials, especially at low pH. The low-frequency component of BHA at pH 5 (at 1,635–1,640 cm^{-1}, normally assigned to β-structures) is also slower than the other components, i.e., it consists of two components with time constants of 83 min (40%) and 357 min (60%). These results indicate that the HA_1 chain becomes more rigid, when bound to membranes alone or in the context of BHA at low pH. A possibility is that HA_1 aggregates on the membrane surface, which could also explain the poorer quality of the H/D exchange data of this molecule. Since HA_1 also perturbs the bilayer interface (see below), it could contribute to membrane fusion by segregating appropriate (e.g., negatively charged) lipids to which it binds in the fusion pore complex. Although conjecture at this point, a role for HA_1-lipid interactions in membrane fusion remains intriguing and should be the subject of future studies.

BHA perturbs the interfacial region of the lipid bilayer

ATR-FTIR spectroscopy, using polarized or unpolarized light, also provides a convenient probe-free measure of perturbations of the lipid bilayer structure by membrane-bound proteins (Tamm & Tatulian, 1997). Here, we asked whether BHA, BHA_2, and HA_1 change the lipid bilayer structure in a way that could be measured by FTIR spectroscopy. We specifically looked for changes in the positions, shapes, and dichroic ratios of the methylene stretching and carbonyl stretching vibrations as a function of protein adsorption. These two bands report on different regions in the lipid bilayer, namely the hydrophobic core and the interfacial regions. None of the protein species studied significantly affected the position or order parameter of methylene stretching vibration. However, BHA and HA_1, but not BHA_2, affected the environment and dynamic structure of the lipid ester carbonyl groups in the bilayer interface. BHA altered the band shape and the order parameter of this vibration and HA_1 exerted a noticeable effect on the band contour, but not on the order parameter.

Our results, that BHA primarily perturbs the interfacial (headgroup) region of target membranes, is consistent with the notion that the fusion peptide predominantly locates into this region of the bilayer (Tsurodome et al., 1992) where it is inserted at an oblique angle (Gray et al., 1996). The primary energetic barrier to close apposition of two membranes and their subsequent fusion is removal of ordered water at distances below $\sim$1 nM from the membrane surface (Rand & Parsegian, 1989; Leckband et al., 1993; Lee & Lentz, 1997). The spectral changes in the lipid carbonyl band contour observed in Figure 7 can arise from two different effects: (1) a change in the relative contributions from hydrated and unhydrated carbonyl groups, which give rise to this band, which is composed of two components at $\sim$1,740 and $\sim$1,724 cm^{-1} for dehydrated and hydrated carbonyls, respectively (Blume et al., 1988; Lewis et al., 1994); and (2) changes in the bandwidth or wavenumber position of these component bands. When we fit the contours of the bands of Figure 7 with two components, each centered at the two observed minima of the corresponding second derivative spectra, we found that for the case of HA_1 the wavenumbers of the two component bands decreased monotonically through a range of about 2 cm^{-1} as a function of increasing protein:lipid ratio (data not shown). In comparison, BHA increased the wavenumbers of the higher frequency carbonyl band and decreased the wavenumbers of the lower frequency carbonyl band monotonically through a range of 3.8 and 2.3 cm^{-1}, respectively, as a function of increasing protein:lipid ratio. Neither the bandwidths nor their relative contributions to the total integrated area of the lipid carbonyl band changed significantly in this analysis.

The decreases of the dichroic ratios of the carbonyl stretching bands (see Table 3) imply a relatively small tilt of the lipid ester carbonyl groups toward the plane of the membrane, which in turn could change the interfacial properties of the bilayer, including hydration and, possibly, the dipole potential. However, the observed changes are barely above, and sometimes below,

the significance level of our measurements. The largest change is seen after binding of BHA, and subsequently lowering the pH to 5, in which case the order parameter decreased from −0.03 to −0.19. In contrast, HA_1 and BHA_2, which together compose BHA, did not significantly affect this parameter. Therefore, the effects of HA_1 and BHA_2 on the lipid carbonyl bond order are not additive. What emerges, then, is an interesting situation where BHA and HA_1 differentially affect the carbonyl groups in the interfacial region of the target bilayer. HA_1 alone appears to primarily affect the state of hydration at the membrane interface, whereas BHA additionally affects the stereochemistry of the lipid ester carbonyl groups.

We, and others, have previously studied the effect of synthetic fusion peptides on the lipid bilayer structure. For example, we observed that synthetic fusion peptides modeled after the N-terminal 23 residues of the influenza HA_2 chain increase the lipid acyl chain order quite dramatically (Gray et al., 1996). In contrast, none of the BHA fragments studied here significantly affect the measured lipid acyl chain order (Table 3). Possible reasons for this discrepancy are that (1) the highest fusion peptide:lipid ratios that could be achieved with the synthetic peptides were much higher than the highest densities achieved with BHA and, therefore, that possible effects of BHA on the lipid acyl chain order are lost in the signal from a large excess of unaffected lipids; and (2) isolated fusion peptides may interact differently with lipid bilayers than fusion peptides in the context of the full protein. For example, when fusion peptides are inserted from BHA, they presumably interact only with the outer leaflet of the bilayer, but when mixed with lipid as synthetic peptides, they may penetrate more deeply and interact with both leaflets of the bilayer.

In summary, the work presented here and previously (Gray & Tamm, 1997) introduces a new perspective on the interaction of influenza HA and its fragments with target membranes. Measurements of pH-dependent secondary structure changes indicate that the conformational change of HA, which is bound to target membranes consists of reversible and irreversible components. The reversible components involve transitions of β-structure, which can be attributed to the HA_1 subunit. Low pH also increases the tilt angle from the membrane normal of both HA and BHA, indicating that two hinges exist near the two membrane attachment points of HA, one near the viral and the other near the target membrane, respectively. The tilting of HA requires HA_1 in both cases. While the dynamic structure of the HA_1 subunit rigidifies, most of the HA molecule, i.e., particularly the HA_2 subunit, becomes more dynamic and perhaps more flexible at fusion pH. HA, and to a lesser degree HA_1, appears to influence hydration at the interface of the target lipid bilayer, which together with the described mechanical and dynamical changes of HA is thought to constitute key ingredients of the mechanism of HA-mediated membrane fusion.

Materials and methods

Materials

The recombinant influenza strain X:31 was propagated in the allantoic cavity of chick embryos and purified as described by Hinterdorfer et al. (1994). POPC and POPG (Na salt) were purchased from Avanti Polar Lipids (Alabaster, Alabama), D_2O from Cambridge Isotope Laboratories (Woburn, Massachusetts), trypsin (type XIII from bovine pancreas), and TLCK and Sephadex G-25 from Sigma (St. Louis, Missouri). All other chemicals were obtained from Fisher (Fair Lawn, New Jersey) or Eastman Kodak (Rochester, New York).

Purification of BHA, BHA_2, and HA_1

BHA was prepared as described previously (Brand & Skehel, 1972). Briefly, freshly thawed virus was incubated with bromelain (~2–5 and 2 mg/mL, respectively) for 16–24 h at 37 °C with shaking. The viral membrane and nucleocapsid were removed through ultracentrifugation (120,000 *g*, 1 h, 4 °C), and the BHA was purified on a 5–20% continuous sucrose gradient (34 K rpm, SW55Ti rotor, 16 h, 4 °C), typically eluting near the middle of the gradient. Removal of contaminant bands was verified by SDS-PAGE analysis under reducing conditions. Sucrose was removed from the BHA-containing fractions by Sephadex G-25 spin column chromatography. Pure BHA, before and after sucrose removal, displayed two bands with apparent molecular masses of 52 and 23 kDa, corresponding to HA_1 and BHA_2, respectively.

Fragments of BHA were obtained by limited trypsinization. Trypsin recognizes four sites in acidified BHA preparations, namely HA_1 at positions 27 and 224 and HA_2 at positions 25 and 39 (Skehel et al., 1982; Ruigrok et al., 1986, 1988). The distribution of proteolytic products is exquisitely sensitive to pH and moderately sensitive to time and enzyme:substrate ratio. When, after 10–15 min prior acidification (citrate buffer, 150 mM citric acid, pH 3.5) of the BHA preparations, the pH of the sample was increased to 6.0–6.5 with Tris (1.0 M, pH 8.0) and trypsin (in working buffer, WB, 5 mM HEPES, pH 7.4, 150 mM NaCl) was added at enzyme:substrate ratios of between 1:25 and 1:40 and incubated at room temperature for 10–30 min, two fragments were produced: HA_1 and BHA_2, which include the fusion peptide. When the pH was increased to 7.5–8, the sites in the fusion peptide region of the HA_2 subunit became accessible, in addition to the HA_1 sites, yielding the $TBHA_2$ fragment whose crystal structure was solved (Bullough et al., 1994). [Treatment with trypsin at this higher pH produces the same fragment as treatment with thermolysin (Ruigrok et al., 1988).] Digestion with trypsin was quenched with a fivefold molar excess of the trypsin inhibitor TLCK and the products were analyzed by SDS-PAGE under reducing conditions. BHA and its proteolytic fragments BHA_2 and HA_1 were separated by sucrose density gradient centrifugation (5–25% continuous gradient on a 40% cushion, SW55Ti rotor, 38 K rpm, 16–18 h, 4 °C). BHA_2 fragments segregated at the 25/40% interface, HA_1 fragments at ~10–15% sucrose, and subfragments HA_1, 28–224 and HA_1, 225–324, at the 0/5% interface. When the trypsin reaction product $TBHA_2$ was loaded onto this sucrose gradient, it migrated to ~5–10% sucrose, i.e., between the HA_1 and HA_1 subfragments. The purified BHA fragments were stored as sucrose gradient fractions at 4 °C for up to 7 days prior to use and were diluted with WB prior to injection into the ATR-FTIR measuring cell.

Preparation of unilamellar lipid vesicles

Unilamellar vesicles for the preparation of supported lipid bilayers were made by drying 800 nmol total lipid dissolved in $CHCl_3$ under a stream of N_2 and then in a high vacuum for at least 1.5 h. The lipids were dispersed in 0.5 mL WB by vortexing, and this dispersion was subjected to repeated freeze-thawing followed by 11–15 cycles of extrusion through a pair of 100 nM pore size polycarbonate membranes (Nucleopore, Pleasanton, California) using a Liposofast syringe-type extruder (Avestin, Ottawa, Canada).

Preparation of supported bilayers

Phospholipid bilayers supported on germanium internal reflection plates (50 × 20 × 1 mm^3 with 45° beveled edges, Spectral Systems, Hopewell Junction, New York) were prepared as described (Frey & Tamm, 1991; Tamm & Tatulian, 1993). Briefly, a POPC monolayer film was deposited onto the argon plasma-cleaned germanium plate from a Langmuir trough held at a constant surface pressure of 36 mN/m and the plate was assembled in a measuring cell. A volume of ~0.8 mL of 1 mM extruded unilamellar liposomes of POPC:POPG (4:1 or 1:1) in WB was injected into the measuring cell so that both surfaces of the monolayer-covered germanium plate were exposed to liposomes. The cell was incubated at room temperature for 2 h to allow for the self-assembly of one supported lipid bilayer on either side of the germanium plate (Hinterdorfer et al., 1994). Excess unfused vesicles were flushed with 5–6 mL (approximately eight measuring cell volumes) D_2O buffer of the appropriate pH (10 mM MES, 5 mM HEPES, 135 mM NaCl; pH adjusted with NaOH in D_2O). For some of the experiments, FTIR spectra of the pure lipid bilayers were recorded at pH 7.4 and 5.0 prior to the addition of protein. In such cases, WB (2.5–3 mL) was flushed after spectra of the bilayers had been recorded and before the protein was incubated. After the protein had been incubated for 10–15 min at pH 7.4, the cell was again flushed with an excess of D_2O buffer, pH 7.4, and the FTIR spectra were measured.

Infrared spectroscopy

Infrared spectra were recorded on a Nicolet 740 Fourier-transform infrared spectrometer as described (Tamm & Tatulian, 1993). The instrument was purged with dry air for 2 h to remove atmospheric H_2O vapor. PATR-FTIR spectra of supported bilayers were recorded with parallel and perpendicular polarized infrared light using a goldwire grid polarizer (Perkin-Elmer, Beaconfield, United Kingdom). Seven hundred fifty to 1,000 interferograms were collected at each polarization with a nominal resolution of 2 cm^{-1}. PATR-FTIR spectra of D_2O buffers of respective pH and polarization (or, in some cases as indicated, spectra of pure lipid bilayers) were used as references in converting single-beam spectra to transmittance and absorbance spectra. For the hydrogen/deuterium (H/D) exchange experiments, the wire grid polarizer was removed and 170 interferograms were co-added at each time point. ATR-FTIR spectra of corresponding buffers, measured under similar conditions (i.e., without the polarizer and at distributed time points), but in the absence of supported bilayers, were used as references.

Processing of FTIR spectra

PATR-FTIR spectra were processed using the Lab Calc software (Galactic Industries, Salem, New Hampshire). If necessary, absorbance due to residual water vapor was subtracted. The baselines were corrected and, when necessary, the amide I′ absorbance spectra were minimally smoothed with a Savitsky–Golay algorithm. To calculate difference spectra, the integrated amide I′ absorbancies were multiplied by a factor to ensure a normalized, constant absolute amide I′ absorbance, from which the spectrum representing the most deuterated state measured at 22 h was subtracted. This normalization was necessary because the absolute amide I′ absorbance varied over time in the H/D exchange experiments. (A decrease of about 10% in the amide I′ intensity over a time course of 22 h was typical in these experiments.)

Order parameters

Order parameters, defined as $S = (3\langle\cos^2\theta\rangle - 1)/2$, were calculated from the measured dichroic ratios, $R^{ATR} = A_{\parallel}/A_{\perp}$ (each integrated between 1,700 and 1,600 cm^{-1}), using the equation

$$S_{oH} = \frac{2(E_x^2 - R^{ATR}E_y^2 + E_z^2)}{f_H(3\cos^2\alpha - 1)(E_x^2 - R^{ATR}E_y^2 - 2E_z^2)} \quad (1)$$

(Frey & Tamm, 1991). $E_{x,y,z}$ are the Cartesian components of the electric field amplitude at the germanium-buffer interface and depend on the refractive indices of germanium (4.0), buffer (1.33), and the supported lipid bilayer (1.43) (Tamm & Tatulian, 1997). The angle α between the α-helix and the amide I transition dipole moment is taken as 39° (Tsuboi, 1962). To determine lipid order parameters, the usual thin film approximation was used. Since the bound proteins reside mainly in the aqueous phase adjacent to the bilayer, the two-phase model (ignoring the dielectric of the lipid bilayer) was used to determine protein order parameters. If one assumes that only the oriented helices in the molecule contribute to the measured nonrandom dichroism, one can scale the order parameter by f_H, i.e., the fraction of residues in oriented helices, and thus obtain the order parameter S_{oH} for the oriented helices. Since in BHA and $TBHA_2$ the major oriented helices are close to parallel to the symmetry axis of the trimer, by measuring S_{oH} one also knows the approximate orientational order of the HA molecules (Tatulian et al., 1995).

H/D exchange kinetics

The amide H/D exchange data were analyzed at selected wavenumbers using a multi-exponential decay function representing the number of residues (measured as difference absorbance) that exchange amide hydrogens for deuteriums as a function of time:

$$\Delta A = \sum_i a_i \exp(-k_i t) \quad (2)$$

where k_i are the rate constants for the H/D exchange of different classes of amide groups and the amplitudes a_i are proportional to the relative fractions of each class of amide hydrogens. The time courses of the amide H/D exchange were fit to Equation 1 using $i = 1$ or $i = 2$ with the NONLIN least-squares fitting program (Johnson & Frasier, 1985; Straume & Johnson, 1992). This program uses the Nelder–Mead simplex algorithm for parameter estimation (Nelder & Mead, 1965). An F-test was performed on pairwise fits ($i = 1$ and 2) to decide whether a double-exponential fit was statistically justified and preferred over a single exponential fit for each data set.

Acknowledgments

This work was supported by grants RO1 AI30557 and T32 GM08323 from the National Institutes of Health. We thank Mr. Dennis Rinehart for expert technical assistance, and Ms. Barbara Nordin for her help in preparing the manuscript. Dr. Suren Tatulian is acknowledged for his contributions and helpful discussions, and Dr. Steve Wharton for advice on the preparation of the trypsin fragments.

References

Bizebard T, Gigant B, Rigolet P, Rasmussen B, Liat O, Bösecke P, Wharton SA, Skehel JJ, Knossow M. 1995. Structure of influenza virus haemagglutinin complexed with a neutralizing antibody. *Nature 376*:92–94.

Blume A, Hübner W, Messner G. 1988. Fourier transform infrared spectroscopy of $^{13}C{=}O$-labeled phospholipids hydrogen bonding to carbonyl groups. *Biochemistry 27*:8239–8249.

Blumenthal R, Sarkar DP, Durell S, Howard DE, Morris SJ. 1996. Dilation of the influenza hemagglutinin fusion pore revealed by the kinetics of individual cell-cell fusion events. *J Cell Biol 135*:63–71.

Brand CM, Skehel JJ. 1972. Crystalline antigen from the influenza virus envelope. *Nature New Biol 238*:145–147.

Bullough PA, Hughson FM, Skehel JJ, Wiley DC. 1994. Structure of influenza haemagglutinin at the pH of membrane fusion. *Nature 371*:37–43.

Chan DC, Fass D, Berger JM, Kim PS. 1997. Core structure of gp41 from the HIV envelope glycoprotein. *Cell 89*:263–273.

Chen J, Wharton SA, Weissenhorn W, Calder LJ, Hughson FM, Skehel JJ, Wiley DC. 1995. A soluble domain of the membrane-anchoring chairn of influenza hemagglutinin (HA_2) folds in *Escherichia coli* into the low-pH-induced conformation. *Proc Natl Acad Sci USA 92*:12205–12209.

Chernomordik L, Kozlov MM, Zimmerberg J. 1995. Lipids in biological membrane fusion. *J Membr Biol 146*:1–14.

Danieli T, Pelletier SL, Henis YI, White JM. 1996. Membrane fusion mediated by the influenza virus hemagglutinin requires the concerted action of at least three hemagglutinin trimers. *J Cell Biol 133*:559–569.

Daniels RS, Downie JC, Hay AJ, Knossow M, Skehel JJ, Wang ML, Wiley DC. 1985. Fusion mutants of influenza virus hemagglutinin glycoprotein. *Cell 40*:431–439.

Doms RW, Helenius A, White J. 1985. Membrane fusion activity of the influenza virus hemagglutinin. The low pH-induced conformational change. *J Biol Chem 260*:2973–2981.

Durrer P, Galli C, Hoenke S, Corti C, Glück T, Vorherr T, Brunner J. 1996. H^+-induced membrane insertion of influenza virus hemagglutinin involves the HA2 amino-terminal fusion peptide but not the coiled coil region. *J Biol Chem 271*:13417–13421.

Englander SW, Mayne L. 1992. Protein folding studied using hydrogen-exchange labeling and two-dimensional NMR. *Annu Rev Biophys Biomol Struct 21*:243–265.

Fass D, Harrison SC, Kim PS. 1996. Retrovirus envelope domain at 1.7 Å resolution. *Nature Struct Biol 3*:465–469.

Frey S, Tamm LK. 1991. Orientation of melittin in phospholipid bilayers. A polarized attenuated total reflection infrared study. *Biophys J 60*:922–930.

Gething MJ, Doms RW, York D, White J. 1986. Studies on the mechanism of membrane fusion: Site-specific mutagenesis of the hemagglutinin of influenza virus. *J Cell Biol 102*:11–23.

Godley L, Pfeifer J, Steinhauer D, Ely B, Shaw G, Kaufmann R, Suchanek E, Pabo C, Skehel JJ, Wiley DC, Wharton S. 1992. Introduction of intersubunit disulfide bonds in the membrane-distal region of the influenza hemagglutinin abolishes membrane fusion activity. *Cell 68*:635–645.

Gray C, Tamm LK. 1997. Structural studies on membrane-embedded influenza hemagglutinin and its fragments. *Protein Sci 6*:1993–2006.

Gray C, Tatulian SA, Wharton SA, Tamm LK. 1996. Effect of the N-terminal glycine on the secondary structure, orientation, and interaction of the influenza hemagglutinin fusion peptide with lipid bilayers. *Biophys J 70*:2275–2286.

Heimburg T, Schuenemann J, Weber K, Geisler N. 1996. Specific recognition of coiled coils by infrared spectroscopy: Analysis of the three structural domains of type III intermediate filament proteins. *Biochemistry 35*:1375–1382.

Hinterdorfer P, Baber G, Tamm LK. 1994. Reconstitution of membrane fusion sites. A total internal reflection fluorescence microscopy study of influenza hemagglutinin-mediated membrane fusion. *J Biol Chem 269*:20360–20368.

Jackson M, Mantsch HH. 1995. The use and misuse of FTIR spectroscopy in the determination of protein structure. *Crit Rev Biochem Mol Biol 30*:95–120.

Johnson ML, Frasier SG. 1985. Nonlinear least-squares analysis. *Meth Enzymol 117*:301–342.

Kemble GW, Bodian DL, Rose J, Wilson IA, White JM. 1992. Intermonomer disulfide bonds impair the fusion activity of influenza virus hemagglutinin. *J Virol 66*:4940–4950.

Kim C-H, Macosko JC, Yu UG, Shin Y-K. 1996. On the dynamics and conformation of the HA2 domain of the influenza virus hemagglutinin. *Biochemistry 35*:5359–5365.

Korte T, Ludwig K, Krumbiegel M, Zirwer D, Damaschun G, Herrmann A. 1997. Transient changes of the conformation of hemagglutinin of influenza virus at low pH detected by time-resolved circular dichroism spectroscopy. *J Biol Chem 272*:9764–9770.

Krimm S, Bandekar J. 1986. Vibrational spectroscopy and conformation of peptides, polypeptides, and proteins. *Adv Prot Chem 38*:181–364.

Leckband DE, Helm CA, Israelachvili J. 1993. Role of calcium in the adhesion and fusion of bilayers. *Biochemistry 32*:1127–1140.

Lee J, Lentz BR. 1997. Evolution of lipidic structures during model membrane fusion and the relation of this process to cell membrane fusion. *Biochemistry 36*:6251–6259.

Lewis RNAH, McElhaney RN, Pohle W, Mantsch HH. 1994. Components of the carbonyl stretching band in the infrared spectra of hydrated 1,2-diacylglycerolipid bilayers: A reevaluation. *Biophys J 67*:2367–2375.

Marsh D. 1997. Dichroic ratios in polarized Fourier transform infrared for nonaxial symmetry of β-sheet structures. *Biophys J 72*:2710–2718.

Nelder JA, Mead R. 1965. A simplex method for function minimization. *Comput J 7*:308–313.

Qiao H, Pelletier SL, Hoffman L, Hacker J, Armstrong RT, White J. 1998. Specific single or double proline substitutions in the "spring-loaded" coiled-coil region of the influenza hemagglutinin impair or abolish membrane fusion activity. *J Cell Biol 141*:1335–1347.

Rand RP, Parsegian VA. 1989. Hydration forces between phospholipid bilayers. *Biochim Biophys Acta 988*:351–376.

Reisdorf WC, Krimm S. 1996. Infrared amide I′ band of the coiled coil. *Biochemistry 35*:1383–1386.

Rodionova NA, Tatulian SA, Surrey T, Jähnig F, Tamm LK. 1995. Characterization of two membrane-bound forms of Omp A. *Biochemistry 34*:1921–1929.

Ruigrok RWH, Aitken A, Calder LJ, Martin SR, Skehel JJ, Wharton SA, Weis W, Wiley DC. 1988. Studies on the structure of the influenza virus hemagglutinin at the pH of membrane fusion. *J Gen Virol 69*:2785–2795.

Ruigrok RWH, Wrigley NG, Calder LJ, Cusack S, Wharton SA, Brown EB, Skehel JJ. 1986. Electron microscopy of the low pH structure of influenza virus haemagglutinin. *EMBO J 5*:41–49.

Skehel JJ, Bayley PM, Brown EB, Martin SR, Waterfield MD, White JM, Wilson IA, Wiley DC. 1982. Changes in the conformation of influenza virus hemagglutinin at the pH optimum of virus-mediated membrane fusion. *Proc Natl Acad Sci USA 79*:968–972.

Steinhauer DA, Martin J, Lin YP, Martin SA, Oldstone MB, Skehel JJ, Wiley DC. 1996. Studies using double mutants of the conformational transitions in influenza hemagglutinin required for its membrane fusion activity. *Proc Natl Acad Sci USA 93*:12873–12878.

Steinhauer DA, Wharton SA, Skehel JJ, Wiley DC. 1995. Studies of the membrane fusion activities of fusion peptide mutants of influenza virus hemagglutinin. *J Virol 69*:6643–6651.

Straume M, Johnson ML. 1992. Monte Carlo method for determining complete confidence probability distributions of estimated model parameters. *Meth Enzymol 210*:117–128.

Surewicz WK, Mantsch HH, Chapman D. 1993. Determination of protein secondary structure by Fourier transform infrared spectroscopy. *Biochemistry 32*:7720–7726.

Tamm LK, Tatulian SA. 1993. Orientation of functional and nonfunctional PTS permease signal sequences in lipid bilayers. A polarized attenuated total reflection infrared study. *Biochemistry 32*:7720–7726.

Tamm LK, Tatulian SA. 1997. Infrared spectroscopy of proteins and peptides in lipid bilayers. *Quart Rev Biophys 30*:365–429.

Tatulian SA, Hinterdorfer P, Baber G, Tamm LK. 1995. Influenza hemagglutinin assumes a tilted conformation during membrane fusion as determined by attenuated total reflection FTIR spectroscopy. *EMBO J 14*:5514–5523.

Tatulian SA, Tamm LK. 1996. Reversible pH-dependent conformational change of reconstituted influenza hemagglutinin. *J Mol Biol 260*:312–316.

Tsuboi M. 1962. Infrared dichroism and molecular conformation of α-form poly-γ-benzyl-L-glutamate. *J Polymer Sci 59*:139–153.

Tsurodome M, Glück R, Graf R, Falchetto R, Schaller U, Brunner J. 1992. Lipid interactions of the humagglutinin HA2 NH_2-terminal segment during influenza virus-induced membrane fusion. *J Biol Chem 267*:20225–20232.

Weissenhorn W, Dessen A, Harrison SC, Skehel JJ, Wiley DC. 1997. Atomic structure of the ectodomain from HIV-1 gp41. *Nature 387*:426–430.

Wharton SA, Ruigrok RWH, Martin SR, Skehel JJ, Bayley PM, Weis W, Wiley DC. 1988. Conformational aspects of the acid-induced fusion mechanism of influenza virus hemagglutinin. Circular dichroism and fluorescence studies. *J Biol Chem 263*:4474–4480.

White JM, Wilson IA. 1987. Anti-peptide antibodies detect steps in a protein conformational changes: Low pH-activation of the influenza virus hemagglutinin. *J Cell Biol 105*:2887–2896.

Wilson IA, Skehel JJ, Wiley DC. 1981. Structure of the haemagglutinin membrane glycoprotein of influenza virus at 3 A resolution. *Nature 289*:366–373.

Appendix

To allow for a better comparison between the analysis of the H/D exchange kinetics of the soluble HA fragments presented here with the corresponding data on the membrane-embedded fragments stud-

ied by Gray and Tamm (1997), we reevaluated our previous kinetic data using the same, more rigorous statistical approach that was used in the present publication. These data, which now include amplitudes for each component and confidence intervals for all fit parameters, are presented in Table A1. The conclusions of Gray and Tamm (1997) are unchanged by this reevaluation.

Table A1. *Analysis of the amide H/D exchange behavior of HA and THA_2 at neutral and low pH at three selected frequencies by fits of the data of Figure 8 of Gray and Tamm (1997) to double (or single) exponential functions*[a]

	1,679 cm^{-1}		1,664 cm^{-1}		1,631 cm^{-1}	
	a_1 (mOD) k_1 ($\times 10^2$ min^{-1})	a_2 (mOD) k_2 ($\times 10^3$ min^{-1})	a_1 (mOD) k_1 ($\times 10^2$ min^{-1})	a_2 (mOD) k_2 ($\times 10^3$ min^{-1})	a_1 (mOD) k_1 ($\times 10^2$ min^{-1})	a_2 (mOD) k_2 ($\times 10^3$ min^{-1})
HA						
pH 7.4						
Amplitude	3.0 (3.0, 3.1)[b]	1.1 (1.0, 1.2)	2.8 (2.8, 2.9)	1.2 (1.1, 1.3)	−1.8 (−1.8, −1.9)	−0.5 (−0.4, −1.0)
Rate	11.4 (9.4, 14.0)	2.2 (2.1, 2.3)	10.8 (9.2, 12.9)	2.2 (2.1, 2.3)	24.6 (11.2, 65.4)	1.3 (1.2, 1.4)
pH 5.0						
Amplitude	3.0 (2.9, 3.0)	1.4 (1.3, 1.5)	2.6 (2.6, 2.7)	1.2 (1.1, 1.3)	−2.4 (−2.3, −2.4)	−2.5 (−2.4, −2.6)
Rate	16.2 (14.1, 18.5)	2.9 (2.8, 3.0)	10.9 (9.5, 12.9)	3.5 (3.3, 3.6)	17.5 (15.9, 19.1)	2.2 (2.1, 2.3)
pH 5.0 + ves.[c]						
Amplitude	2.3 (2.3, 2.4)	1.1 (1.0, 1.3)	1.9 (1.7, 1.9)	1.1 (1.0, 1.2)	−3.1 (−3.0, −3.2)	−2.3 (−2.1, −2.5)
Rate	17.0 (13.8, 21.3)	2.6 (2.5, 2.7)	12.4 (9.9, 15.0)	3.3 (3.1, 3.5)	13.8 (11.6, 16.2)	2.3 (2.2, 2.4)
THA_2						
pH 7.4						
Amplitude	1.1 (1.1, 1.2)	0.8 (0.7, 0.9)	1.6 (1.5, 1.6)	0.8 (0.8, 0.9)	—	−1.5 (−1.5, −1.6)
Rate	6.3 (5.3, 7.3)	2.0 (1.9, 2.1)	6.1 (5.5, 7.0)	3.9 (3.8, 4.1)	—	1.3 (1.1, 1.4)
pH 5.0						
Amplitude	2.5 (2.5, 2.5)	1.1 (1.0, 1.1)	1.6 (1.6, 1.6)	1.0 (0.9, 1.0)	−3.2 (−3.0, −3.2)	−1.0 (−0.9, −1.2)
Rate	10.2 (9.1, 11.6)	5.8 (5.6, 5.9)	24.0 (21.2, 27.4)	8.8 (8.5, 9.1)	4.5 (3.7, 6.6)	2.0 (1.9, 2.2)
pH 5.0 + ves.[c]						
Amplitude	1.2 (1.1, 1.2)	0.8 (0.8, 0.9)	0.7 (0.6, 0.7)	0.7 (0.7, 0.8)	−3.0 (−2.9, −3.0)	−1.0 (−0.8, −1.1)
Rate	7.8 (6.6, 9.5)	2.8 (2.6, 3.0)	8.2 (6.5, 10.2)	2.6 (2.3, 2.9)	15.8 (11.5, 20.9)	2.4 (2.3, 2.5)

[a]Amplitudes and rate constants were found using the Nelder–Mead simplex algorithm (Johnson & Frasier, 1985).

[b]All numbers in parentheses are the confidence intervals for one standard deviation found using a Monte Carlo simulation with 800 cycles (Straume & Johnson, 1992).

[c]With target vesicles bound.